Available online at www.sciencedirect.com
SCIENCE DIRECT
Catalysis Today 110 (2005) 330–338
CATALYSIS TODAY
www.elsevier.com/locate/cattod

Distribution and properties of catalytically active Cu^{2+}-sites on a mesoporous MCM-41 silicate modified by Al, Zr, W, B, or P ions

A.V. Kucherov [a,*], A.N. Shigapov [b], A.V. Ivanov [a], T.N. Kucherova [a], L.M. Kustov [a]

[a] *Zelinsky Institute of Organic Chemistry, RAS, Leninsky Prosp. 47, Moscow 119991, Russia*
[b] *Scientific Research Laboratory, Ford Motor Company, MD 3179/SRL, P.O. Box 2053, Dearborn, MI 48121, USA*

Abstract

Pure SiO_2 having a MCM-41 structure was modified by the introduction of 1 mmol/g of Al, Zr, W, B, or P. The parent silica and the modified materials were used to support a dispersed cupric oxide. The distribution, properties and thermal stability of the catalytic Cu^{2+}-active sites were examined by ESR and IR spectroscopy and by measuring the activity in a test reaction of ethane oxidation. Modification of the parent silica MCM-41 influences drastically the stabilization of isolated Cu^{2+}-species. Al-MCM-41 provides the most disperse (70–80%) and thermally stable state of the cupric phase. However, no simple correlation exists between the total number of surface Cu^{2+}-sites and the catalytic activity. The specific catalytic activity (per one Cu^{2+}-active site accessible to the reactants) depends strongly on the structure of the localized site. Isolated Cu^{2+}-sites grafted to Al-MCM-41 show relatively high activity for the sample calcined at 520 °C. Thermal treatment at 650–750 °C causes a sharp loss of specific Cu^{2+} catalytic activity of Cu/Al-MCM-41 (as is also the case with CuH-ZSM-5). The less disperse cupric phase in non-modified MCM-41 demonstrates a higher specific catalytic activity.

Keywords: MCM-41; Cu^{2+} active sites; ESR; IR; Ethane oxidation

1. Introduction

Mesoporous molecular sieves with a tubular MCM-41 structure are of interest as SiO_2-based supports because of their larger pore diameter than conventional high-silica zeolites [1–3]. Atomic-scale engineering of catalytic functions in narrow inner voids of high-silica zeolites (ZSM-5, mordenite, ferrierite, beta) having 0.5–0.7 nm channels is restricted to the smallest organic molecules. Previously we studied narrow-channel zeolitic catalysts containing *isolated* transition metal cations as active redox sites [4–11]. Anchoring of catalytically active sites in MCM-41 channels of ~3 nm internal diameter could open the way of preparation of biomimetic catalysts with pore sizes able to accommodate relatively large organic molecules. With that end in view, different triple systems [Cu-organic ligands-MCM-41] were prepared and studied recently [12–20].

On the other hand, different non-organic modifiers can be grafted into the SiO_2-based lattice of MCM-41 to create additional acidic sites for anchoring transition ions as redox catalytic sites. Thus, the high surface and regular porosity of MCM-41 permits to prepare systems with acid, base, and redox catalytic properties potentially useful for a wide number of organic reactions [21–26]. Substantial differences can be expected in the stability, coordination states, and *association* of cupric ions inside MCM-41 channels, as distinct from the ZSM-5 zeolite.

The aim of our work was to examine the behavior of pure and modified SiO_2 with a MCM-41 structure in the stabilization of dispersed cupric ions. ESR and IR examination of these samples permits to assess quantitatively the distribution, properties and thermal stability of surface Cu^{2+}-active centers accessible to gas-phase molecules. Comparison of such samples, with an identical support structure and a large surface

* Corresponding author. Tel.: +709 513 76617; fax: +709 513 55328.
E-mail address: avk@ioc.ac.ru (A.V. Kucherov).

0920-5861/$ – see front matter © 2005 Elsevier B.V. All rights reserved.
doi:10.1016/j.cattod.2005.09.031

area, could establish a correlation between the structure and *specific* catalytic activity of the sites in test reaction of ethane oxidation.

2. Experimental

2.1. Sample preparation

2.1.1. Synthesis of MCM-41

A typical synthesis gel for MCM-41 sample was prepared by adding 94 ml (100 g) of silica sol (15 wt.%, Alfa Aesar) to an aqueous solution containing 21 ml of TEAOH ($(C_2H_5)_4NOH$, 35% solution, Aldrich) and 123 ml of cetyltrimethylammonium chloride CTMA-Cl (25 wt.% solution, Aldrich), with stirring for 30 min. The resulting gel was placed into 250 ml polypropylene bottles, hermetically closed, and heated at 110 °C for 72 h in a heating box, followed by filtration, washing with ethanol and distilled water, and drying at room temperature overnight. Finally, the solid obtained was calcined in air at 540 °C for 18 h. This method of preparation is similar, but not identical, to the described elsewhere [27].

2.1.2. Preparation of Me-MCM-41

MCM-41 modified with Al, Zr, W, B and P ions, further marked as Me-MCM-41, e.g. Al-MCM-41, Zr-MCM-41, etc., were prepared by impregnation of MCM-41 synthesized as described above, with aqueous solutions of aluminum nitrate, zirconium citrate, $H_4SiW_{12}O_{40}$ heteropolyacid, boric acid or H_3PO_4, respectively, with the following drying at room temperature overnight. The samples were then placed in a plug-flow reactor, linearly heated up to 540 °C in a flow of dry air (2 h), and calcined for 18 h. The amount of added component was selected as 1 mmol per 1 g of MCM-41.

2.1.3. Preparation of Cu/Me-MCM-41

As the last step, 1 wt.% of Cu was introduced by incipient wetness impregnation of the parent and modified MCM-41 by a water solution of copper nitrate (99.95% purity) with subsequent drying overnight. Again, the samples were placed in a plug-flow reactor, linearly heated up to 520 °C in a flow of dry air (2 h), and calcined for 4 h. Since the introduced amount of ions was retained by the impregnated samples no further analysis was done.

2.2. Characterization

2.2.1. X-ray diffraction

The XRD measurements were carried out using a Scintag X1 diffractometer with Cu Kα radiation.

2.2.2. Surface area

Surface parameters were determined by nitrogen adsorption–desorption isotherms at −196 °C using a Micromeritics ASAP 2400 instrument. Prior to surface areas measurements, the samples were degassed at 450 °C for 4 h under vacuum (<5 mTorr).

2.2.3. IR spectroscopy

IR spectra were recorded at 20 °C in the diffusion reflectance mode (8 cm^{-1} resolution) using a Nicolet Protege 460 FT-IR spectrometer. Powder samples were placed in a quartz cell with CaF_2 window, activated in O_2 (100 Torr) at 500 °C, and evacuated. The catalytic centers were studied using CO, NO, and CD_3CN as molecular probes. The Kubelka–Munk equation was used for the treatment of the spectra (OMNIC program).

2.2.4. ESR measurements

The ESR spectra were taken in the X-band ($\lambda \cong 3.2$ cm) at 20° and −196 °C on a Bruker ESP300 spectrometer, equipped with a 4104OR cavity and a co-axial quartz Dewar. The ESR signals were registered at microwave power 6.35 mW and modulation amplitude 4.0 G in the field range of 2000–4000 G (10 scans with a sweep time of 42 s). The Bruker ESP300E software and the special Bruker program WIN-EPR (version 901201) were used for data treatment (baseline correction, noise reduction, double integration).

The samples were crushed into 0.1–0.2 mm particles, charges of the sample (39–41 mg) were placed in identical quartz ampoules (3.5 mm diameter), calcined in a furnace at a given temperature, taken out, immediately connected to the vacuum system, evacuated for 2–3 min to 0.03 Torr, and sealed off. Then the ESR-spectra were registered at 20 °C or at −196 °C and normalized for the differences in sample weight.

For quantitative comparison, the copper-containing samples were impregnated with distilled water, kept for 1 h at room temperature, and then the ESR spectra were registered at −196 °C. A water-impregnated 0.5% CuHZSM-5 sample was used as a reference for quantitation. Earlier it was demonstrated that all the copper in this low-loaded zeolitic sample contributes to the Cu^{2+}-ESR signal [5,10]. For highest accuracy, sets of samples were measured consecutively, with ampoules in the same position inside the ESR resonator.

2.3. Catalytic testing

The catalysts were tested in ethane oxidation [28,29] by placing a 92–98 mg charge of the sample, having 0.25–0.5 mm particles, in a fixed-bed quartz microreactor and conditioned at 520 °C by dry air flow (50 cm^3/min) for 2 h. Then the temperature of catalytic run was fixed and the reaction mixture was fed to the reactor under 1 atm pressure and a space velocity of ∼20,000 h^{-1}. Catalyst activities were measured at ethane conversion from 2 to 60% for a mixture of reactants [90.6 vol.% He + 8.4 vol.% O_2 + 0.96 vol.% C_2H_6] which corresponds to a ∼2.5-fold excess of oxygen. Samples of the reactor effluent were injected periodically into a chromatograph. CO_2 and H_2O were the major products in all catalytic runs. Traces of ethene were also detected in some runs, usually at temperatures above 500–520 °C.

After the catalytic testing the catalyst charge was calcined in situ in an air flow at 650 °C for 1 h; at 650 °C for 3 h; at 750 °C for 1 h. Following this treatment the catalytic tests at 400–600 °C were repeated.

Table 1
BET surface area of MCM samples

Sample	BET surface area (m^2/g), after calcinations at 540 °C
MCM-41	1180
Al-MCM-41	1160
Zr-MCM-41	1080
W-MCM-41	960
B-MCM-41	1170
P-MCM-41	1110

3. Results and discussion

3.1. Surface area and structure

X-ray diffraction patterns of calcined MCM-41, Me-MCM-41, and Cu/Me-MCM-41 samples confirm the formation and preservation of a structure typical of the mesoporous MCM-41 molecular sieve. The spectra after calcinations show an intense peak at $2\theta = 2.2^\circ$ corresponding to a spacing of $d_{1\,0\,0} = 4$ nm and indicative of the existence of the hexagonal MCM-41 phase [23,30]. No substantial loss of crystallinity occurs as a result of a long-term sample calcination at 540 °C in dry air.

Table 1 summarizes the surface area data of the samples derived from the BET isotherms. It is seen that introduction of 1 mmol/g of additives and repeat calcinations of samples at 540 °C for 18 h does not cause a substantial decrease of the initial value of the surface area of the mesoporous MCM-41 material.

Only for the W-containing sample the resulting area loss reaches ~15%. Subsequent introduction of 1 wt.% Cu, with further calcinations at 520 °C for 4 h, causes only negligible changes in the surface area.

Thus, the active cupric phase of all the catalysts is dispersed on supports having an identical structure and surface area. This facilitates the direct comparison of adsorption and catalytic properties of the active sites stabilized by surface of starting and modified MCM-41.

3.2. FT-IR measurements

3.2.1. CD_3CN adsorption

Earlier [10,31,32] it was demonstrated that CD_3CN adsorption on copper-containing surfaces causes only a minor change in the state of the ion charge. FT-IR spectra obtained with the use of this test-molecule are presented in Fig. 1 and the data are summarized in Table 2.

In the region of the CN-bond vibration, two main bands, at 2275 and 2316 cm^{-1}, appear after sorption of CD_3CN on Cu/MCM-41 (Fig. 1a). The band at 2275 cm^{-1} corresponds to physical sorption of CD_3CN on free MCM-41 surface, and the second one is typical of CD_3CN adsorbed on Cu^{2+} sites [10,31]. The lack of a band at ~2300 cm^{-1} confirms that the amount of Cu^+ sites in our pre-oxidized sample is negligible.

The use of modified Me-MCM-41 complicates the spectra due to the appearance of additional bands as a result of CD_3CN sorption on acid sites formed by the modifiers (Fig. 1b–d). Deconvolution of the spectra permits to identify bands at 2303 and 2332 cm^{-1} for CD_3CN complexes formed on Zr^{4+} and Al^{3+}, respectively. For the W-containing sample at least two new adsorption sites can be identified, with bands at 2305 and

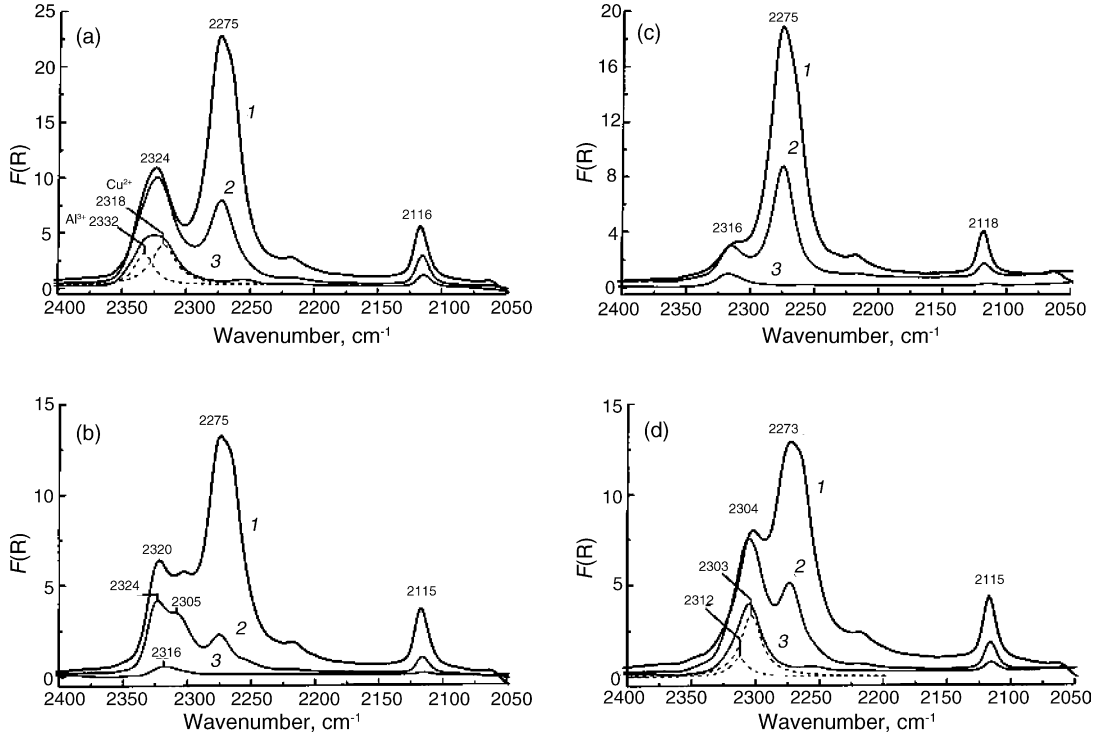

Fig. 1. FT-IR spectra of (a) Cu/MCM-41, (b) Cu/Zr-MCM-41, (c) Cu/Al-MCM-41, and (d) Cu/W-MCM-41 in the region of CN stretching vibration: (1) after adsorption of CD_3CN; (2) after evacuation at 20 °C; (3) after evacuation at 100 °C.

Table 2
Vibration frequencies of the of CN bond in CD_3CN adsorbed on Cu/Me-MCM-41 after evacuation at 100 °C

Samples	νCN (cm^{-1})	Adsorption site
Cu/MCM	2316	Cu^{2+}
Cu/Al-MCM	2332	Al^{3+}
	2318	Cu^{2+}
Cu/Zr-MCM	2303	Zr^{4+}
	2312	Cu^{2+}
Cu/W-MCM	2316	Cu^{2+}

Table 3
Frequencies of the vibration of CO adsorbed on Cu/M-MCM samples

Samples	νCO (cm^{-1})	Adsorption complex
Cu/MCM	2202	Cu^{2+}–CO (?)
	2180, 2153	$Cu^{+}(CO)_2$
	2160	Cu^{+}–CO
	2140	Cu_{ox}^{+}–CO
Cu/Al-MCM	2225	Al^{3+}–CO
	2210	Cu^{2+}–CO (?)
	2180	$Cu^{+}(CO)_2$
	2157	Cu^{+}–CO
Cu/Zr-MCM	2195	Zr^{4+}–CO
	2150	Cu^{+},Cu_{ox}^{+}–CO
Cu/W-MCM	2210	Cu^{2+}–CO (?)
	2175	$Cu^{+}(CO)_2$
	2145	Cu^{+},Cu_{ox}^{+}–CO

2324 cm^{-1}, but CD_3CN bonding on these sites is weak (Fig. 1d). At the same time, an intense band at 2312–2318 cm^{-1} confirms the presence of Cu^{2+} sites in all these samples.

Hence, the use of CD_3CN identifies the Cu(II) valence state as the major one for all the catalysts. The properties of the surface cupric sites were measured in greater detail by using CO and NO as molecular probes.

3.2.2. CO and NO adsorption

FTIR spectra obtained when using CO as a test-molecule are shown in Fig. 2, and vibration frequencies are listed in Table 3.

The spectral region of CO vibration can be sub-divided on three parts: >2190; 2190–2170; 2160–2130 cm^{-1}. According to literature, strong bands with peaks at 2160–2130 cm^{-1} correspond to vibrations of CO adsorbed on Cu^{+} ions in different coordinations [33–36]. Formation of Cu^{+} takes place as a result of Cu^{2+} reduction by CO molecules. Appearance of the band at 2350 cm^{-1}, associated with the CO_2 formed, confirms this assumption. The band at 2140 cm^{-1} is typical of Cu^{+} ions in CuO crystallites, whereas the bands at 2150–2160 cm^{-1} can be attributed to isolated Cu^{+} ions stabilized by the oxide supports [36–39]. If so, the ratio of the band intensities (Fig. 2) can be used for evaluation of copper distribution between different states of aggregation. Dispersion of copper in our samples evaluated by this method decreases in the sequence:

Cu/Al-MCM-41 > Cu/Zr-MCM-41 > Cu/W-MCM-41 > Cu/MCM-41

The vibration region at 2190–2170 cm^{-1} includes bands from CO adsorbed on either Cu^{2+} ions (2180–2190 cm^{-1}) or

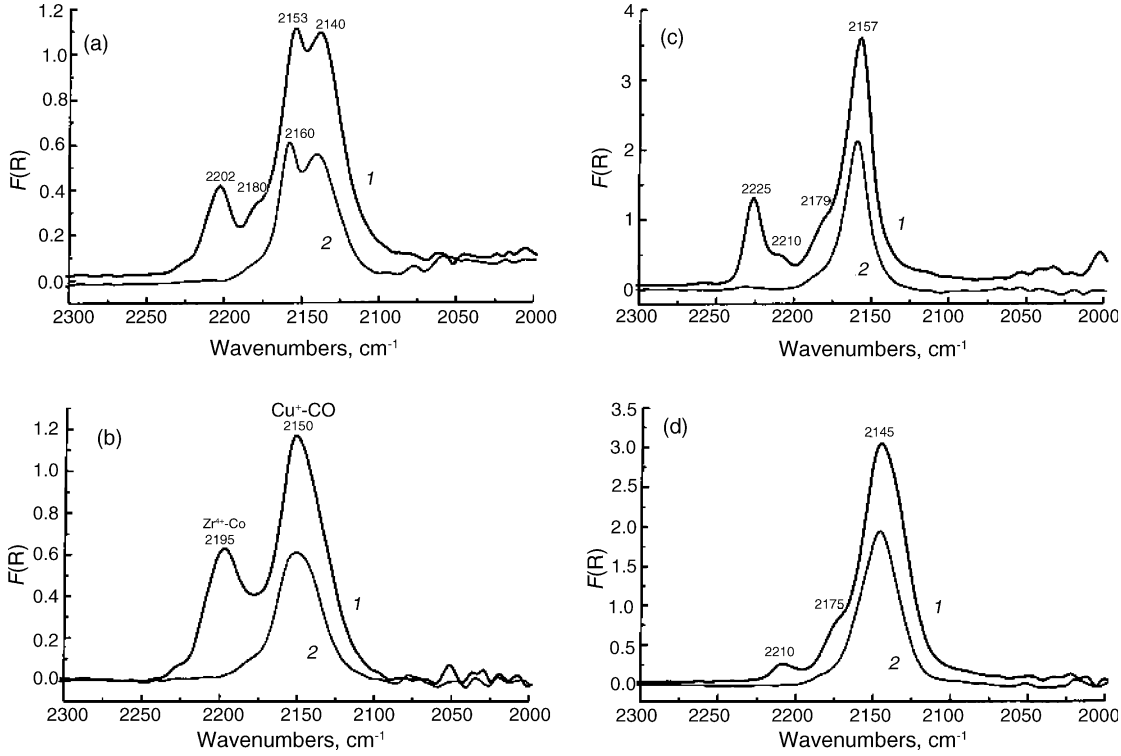

Fig. 2. FT-IR spectra of (a) Cu/MCM-41, (b) Cu/Zr-MCM-41, (c) Cu/Al-MCM-41, and (d) Cu/W-MCM-41 in the region of CO stretching vibration: (1) after adsorption of CO; (2) after evacuation at 20 °C.

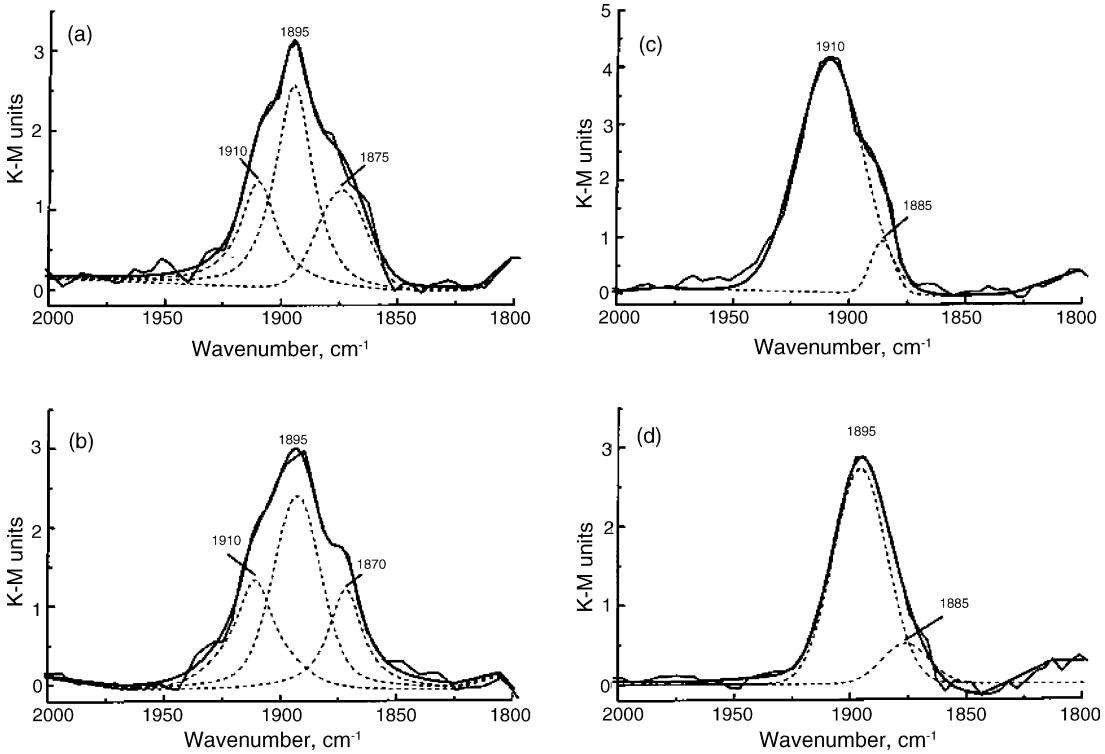

Fig. 3. FT-IR spectra of (a) Cu/MCM-41, (b) Cu/Zr-MCM-41, (c) Cu/Al-MCM-41, and (d) Cu/W-MCM-41 in the region of NO stretching vibration.

Cu^+ ions as dicarbonyls, $Cu^+(CO)_2$, (2175–2180 cm^{-1}) [31,40,41] or 2163 cm^{-1} [34]. It was shown, however, that surface complexes of CO with weakly associated Cu^{2+} ions are formed at low temperature only (163 K), and no complexation at all takes place on Cu^{2+} ions located inside the oxide matrix due to coordinative saturation of copper ions [36]. So, shoulders at 2180 cm^{-1} (Fig. 2) correspond, more likely, to dicarbonylic species $Cu^+(CO)_2$.

Bands at 2195 and 2225 cm^{-1} (Fig. 2b and c) can be attributed to CO complexes with Zr^{4+} and Al^{3+}, respectively. For the system containing W^{6+} ions (WO_3) formation of complexes with CO is not typical. In addition, bands at 2202–2210 cm^{-1} are seen in our spectra (Fig. 2). It was shown earlier that formation of coordinatively unsaturated Cu^{2+} ions as a result of oxygen ligand loss can result in formation of complexes with CO [10]. So, these bands can be indicative of adsorption of CO on defect Cu^{2+} sites. From the comparison of our spectra (Fig. 2) it is clearly seen that a fraction of this type of site/complex on Cu/MCM-41 exceeds substantially those for other three samples, with modified supports.

The analysis of IR spectra of NO adsorbed on Cu/zeolitic systems permits to identify different coordinative and valence states of copper [42,43]. At the same time, it was shown that interaction of NO molecules with Cu(I)-ions can oxidize these sites to Cu^{2+} [44]. NO adsorption on Cu/MCM-41 results in the appearance of an asymmetric band with a maximum at 1895 cm^{-1} (Fig. 3a) corresponding to vibration of NO adsorbed on Cu^{2+}. The absence of bands at 1700–1850 cm^{-1} confirms the lack of Cu^+ state in the pre-oxidized sample. Deconvolution of the spectrum according to [43] gives us three bands at 1910, 1895, and 1875 cm^{-1}, respectively. These bands are indicative of Cu^{2+}-ions in different environments. As was demonstrated before, the band at 1910 cm^{-1} corresponds to isolated Cu^{2+} ions in square-pyramidal coordination [43]. The band at 1895 cm^{-1} can be attributed to NO sorption on $[Cu^{2+}–OH]^+$ sites having a square-planar coordination of the copper, and the low-frequency band at 1875 cm^{-1} is assigned to adsorption on CuO bulk phase [45]. The relative dispersion of copper in our samples can be evaluated from the peak intensities in deconvoluted spectra (Fig. 3). These values are presented in Fig. 4. Cu/MCM and Cu/Zr-MCM contains all three forms of Cu^{2+} in similar proportions. By contrast, Cu/Al-MCM contains mainly isolated square-pyramidal Cu^{2+} ions, with a negligible presence of CuO. The presence of Al^{3+}-sites on the surface of the support provides considerably better dispersion of copper, with the species being similar to the cationic sites in Cu/zeolites

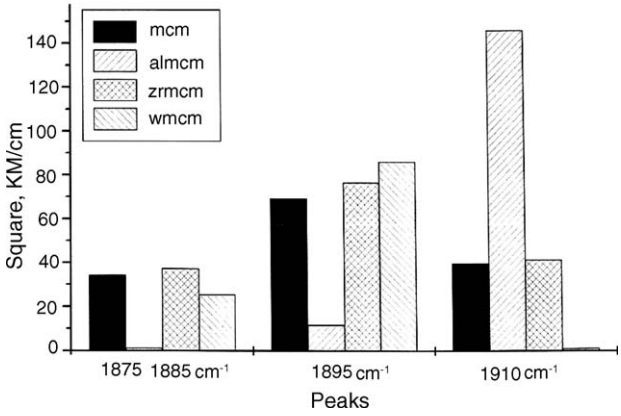

Fig. 4. Relative fractions of NO-complexes on Cu^{2+} sites, calculated from the deconvoluted peaks shown in Fig. 3.

[43]. On the other hand, the Cu/W-MCM sample shows only the presence of aggregated copper states and a complete absence of cationic, isolated copper ions such as are typical in zeolites.

3.3. ESR measurements

The shape and the integral intensity of the Cu^{2+}-ESR signal depend on both ion dispersion and coordination. Pure bulk CuO shows no ESR line from paramagnetic Cu^{2+} ions due to a strong dipole–dipole interaction in the regular crystalline phase. Only dilution of Cu^{2+} ions by the support matrix weakens this interaction and results in appearance of Cu^{2+}-ESR signals from magnetically ''isolated'' ions and/or small clusters (2D-islands) with weakened interaction between Cu^{2+} ions. As to the geometrical distances, a 30–50% increase in [Cu^{2+}–O–Cu^{2+}] bond length is sufficient for substantial weakening of the magnetic interaction, and a 0.8–1 nm distance provides magnetic isolation of the ions. In the ESR spectrum from isolated Cu^{2+} ions four components of a hyperfine splitting (HFS) are always well resolved in the parallel part, with $A_{\|}$ and $g_{\|}$ parameters being sensitive indicators for the symmetry of the local crystal field. Weak clusters of Cu^{2+} usually give relatively broad and unstructured ESR lines. Quantitation of active cupric sites on the support surface from ESR spectra becomes a difficult problem in samples containing mixtures of different states of isolated and interacting Cu^{2+} ions. ESR was used as quite informative method in some recent study of copper-containing MCM-41 but it was done on qualitative level [25,46–48]. The most detailed ESR study of Cu/Ga/MCM-41 and Cu/MCM-41 made by Kevan et al. [48] demonstrates that Cu(II) fully coordinates with a maximum coordination number of polar adsorbates (water and methanol) in MCM-41 mesopores.

In earlier quantitative studies of Cu^{2+} in H-ZSM-5 we have used frozen water solutions of copper salts to prepare a solid specimen with isolated Cu^{2+} ions in hydrate shells well approximating the CuH-ZSM-5 zeolite saturated with H_2O and containing only six-coordinated Cu^{2+} ions [5,10]. It was shown that virtually all the cupric ions in hydrated low-loaded CuH-ZSM-5 are ''ESR-visible''. This approach, with insertion of strong water ligands into the coordinative sphere of accessible Cu^{2+} ions, is used now for quantitation of *surface* Cu^{2+}-sites in Cu/Me-MCM-5 samples.

3.3.1. Quantitative ESR measurements

Fig. 5 shows ESR spectra from dehydrated Cu/MCM-41, Cu/Zr-MCM-41 and Cu/Al-MCM-41 samples taken at room temperature at identical magnification and sample weight. Three other samples demonstrate a weak signal similar to that shown in Fig. 5a. Normalized double integral (DI/N) intensities of these Cu^{2+}-ESR signals, from dry evacuated samples, differ by ~2 orders of magnitude (Fig. 5). The signals cannot be quantified but one can infer that Al-promoted MCM-41 stabilizes a much larger portion of isolated Cu^{2+} ions as compared with Zr-promoted sample. Resolution of HFS components is rather poor but parameters of the parallel part can be estimated as $A_{\|}$ = 158 G, $g_{\|}$ = 2.33 which corresponds to pyramidal symmetry of isolated Cu^{2+} sites.

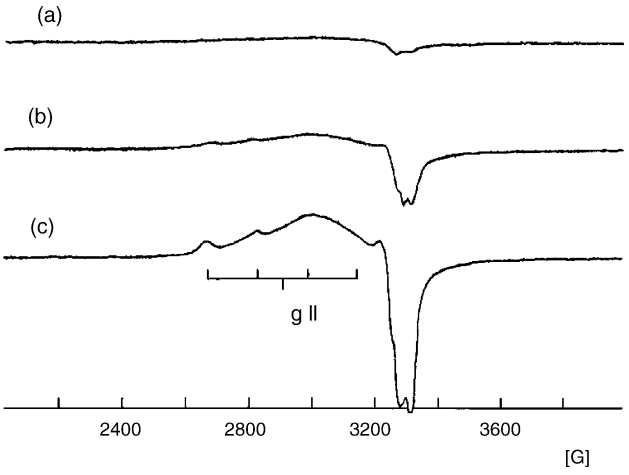

Fig. 5. ESR spectra, taken at 20 °C, of the samples calcined in air at 540 °C, after evacuation: (a) 1%Cu/MCM-41; (b) 1%Cu/Zr-MCM-41; (c) 1%Cu/Al-MCM-41.

A superimposed broad line (Fig. 5c) points to the presence of weakly associated species as well. The amount of isolated Cu^{2+} seems to be negligible in the four other samples. Calcination of all samples at 750 °C for 2 h does not change substantially the Cu^{2+}-ESR spectra: only a ~20% increase in the DI/*N* value takes place for Cu/Al-MCM-41 confirming the high stability of the dispersed cupric state on this support.

Impregnation of precalcined Cu/Me-MCM-41 samples with water sharply changes the shape of the Cu^{2+}-ESR-spectra, and causes a very substantial rise in the intensity. Fig. 6 shows ESR

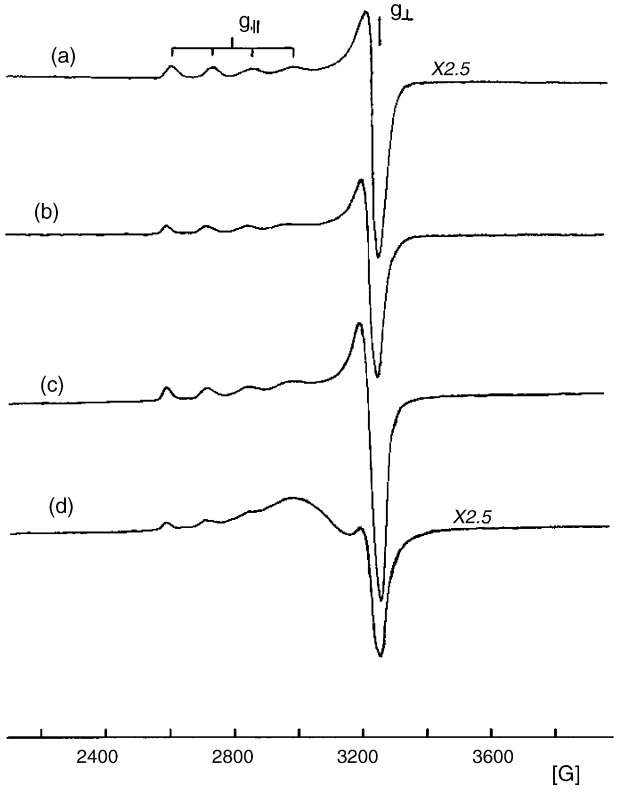

Fig. 6. ESR spectra, taken at −196 °C, of the samples calcined at 540 °C and impregnated by water: (a) 1%Cu/MCM-41; (b) 1%Cu/Zr-MCM-41; (c) 1%Cu/Al-MCM-41; (d) 1%Cu/W-MCM-41.

spectra taken at −196 °C from Cu/MCM-41, Cu/Zr-MCM-41, Cu/Al-MCM-41 and Cu/W-MCM-41 samples, with identical weight, precalcined at 540 °C and impregnated with water. The spectra formed as a result of a strong adsorption of water molecules on cupric sites, with $A_{\|} = 132$ G, $g_{\|} = 2.39$, and $g_{\perp} = 2.08$, indicate that the symmetry of Cu^{2+}-sites approximates the octahedral one. A spectrum similar to that shown in Fig. 6a, was reported by Kevan et al. [48,49] for hydrated Cu/MCM-41. Spectra shown in Fig. 6a–c are identical in shape with the signal from a wet frozen CuH-ZSM-5 sample containing isolated cupric ions only. The signal from Cu/W-MCM-41 (Fig. 6d) contains also a superimposed broad line from interacting Cu^{2+} ions. Fig. 7 shows for comparison ESR spectra taken at −196 °C from the same Cu/MCM-41, Cu/Zr-MCM-41, Cu/Al-MCM-41 and Cu/W-MCM-41 samples but calcined at 750 °C and impregnated with water. Considerable loss of the total intensity can be seen for the Cu/W-MCM-41 sample only (Figs. 6d and 7d).

The integral intensities of spectra increase by one to two orders of magnitude as a result of impregnation with water. The presence of water cannot affect cupric ions either rigidly inserted into the support lattice or associated in small cupric particles with the regular CuO lattice. Thus, the cupric ions under consideration are not rigidly bound to the lattice of the support and are able to attach additional ligands. The strong bonding of H_2O molecules on Cu^{2+}-sites weakens drastically

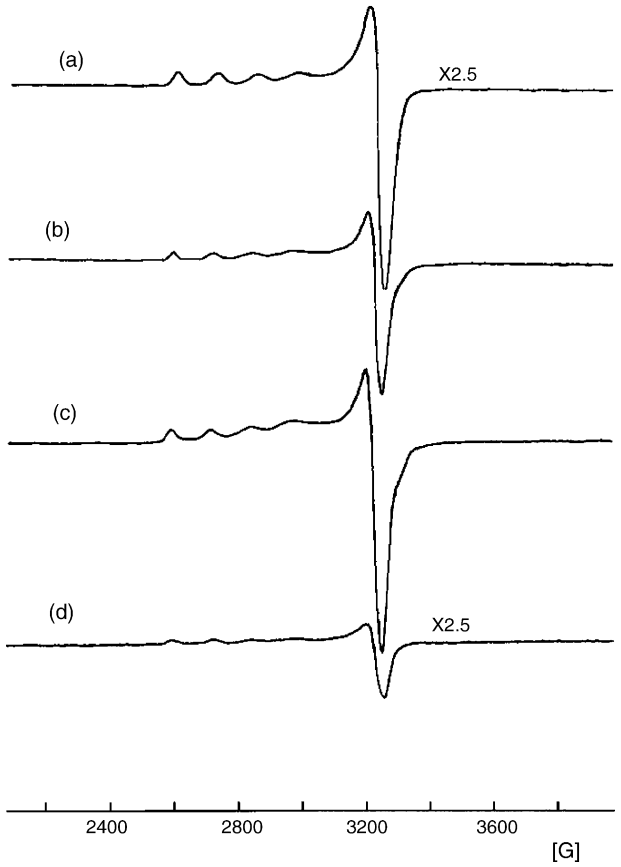

Fig. 7. ESR spectra, taken at −196 °C, of the samples calcined at 750 °C and impregnated by water: (a) 1%Cu/MCM-41; (b) 1%Cu/Zr-MCM-41; (c) 1%Cu/Al-MCM-41; (d) 1%Cu/W-MCM-41.

Table 4
The fraction of the Cu^{2+}-sites coordinated with water molecules on the surface of different Cu/Me-MCM-41 samples, as determined from ESR data

Sample	Dispersion	
	Calcined 520 °C, 4 h	Calcined 750 °C, 2 h
1% Cu/MC-41	0.22	0.22
1% Cu/Zr-MCM-41	0.48	0.42
1% Cu/Al-MCM-41	0.68	0.77
1% Cu/W-MCM-41	0.33	0.07
1% Cu/B-MCM-41	0.62	0.32
1% Cu/P-MCM-41	0.59	0.50

both the spin-lattice interaction of isolated Cu^{2+} sites with support, and [Cu^{2+}–O–Cu^{2+}] interaction in small non-ordered cupric clusters (islands) on the surface of MCM-41 channels. In both instances, the Cu^{2+} ions are readily accessible to H_2O molecules filling the inner MCM-41 voids. Hydration shells effectively separate coupled paramagnetic ions or weaken the spin–lattice interaction of Cu^{2+} with the MCM-41 framework. Thus, direct comparison with a wet CuH-ZSM-5 sample containing a known amount of isolated Cu^{2+} cations permits a selective quantitation of Cu^{2+}-active sites on the surface of MCM-41 supports. Values of the cupric phase dispersion obtained from such a calculation are listed in Table 4.

The lowest dispersion of the cupric phase is observed on non-modified MCM-41 surface but even in this case the fraction of surface Cu^{2+}-sites readily interacting with H_2O molecules is substantial (∼22%). It is known that negatively charged silica species interact with positively charged external surface of the micelles during the synthesis, resulting in ∼20% (Si–OH) groups in the calcined MCM-41 [30]. It follows that ion exchange capacity of these silanol protons can be quite pronounced. We can conclude from the sharp change of the ESR spectrum, caused by hydration of the dry sample (see Figs. 5a and 6a), that the main part of Cu^{2+} surface sites in Cu/MCM-41 belong to small irregular cupric clusters rather than to well separated Cu^{2+} ions. It is surprising, however, that the sample preserves this disperse state of the cupric phase even after thermal treatment at 750 °C (Table 4).

Modification of the starting SiO_2-MCM-41 with Al, Zr, W, B, or P ions results in more or less pronounced increase in the dispersion of copper (Table 4) due to creation/grafting of additional sites for Cu^{2+} anchoring. The strong effect of Si/Al ratio on the dispersion of CuO clusters in MCM-41 was demonstrated earlier [46,51]. Pronounced influence of Zn and Nb on CuO dispersion was also noted [25,52,53]. We also observe the highest Cu^{2+} dispersion on Al^{3+}-modified support where the insertion of the modifier into MCM-41 makes the formation of strong zeolite-like acid sites possible.

As a result, the isolated form of Cu^{2+}-sites becomes dominant for Cu/Al-MCM-41, with ∼2/3 of the copper introduced being accessible to water molecules. These data coincide well with the results of study of low-loaded Cu/Al-MCM-41 samples where virtually only isolated Cu^{2+} ions were detected [46,48,50,51]. Calcination at 750 °C does not lead to any collapse of the support structure and causes even a small increase in the number of the isolated surface Cu^{2+}-sites in Cu/

Al-MCM-41 (Table 4). By contrast, the sample Cu/W-MCM-41, containing interacting clusters with a relatively high starting dispersion of the cupric phase (∼33%), demonstrates low stability during the same high-temperature treatment. The loss of accessible Cu^{2+} sites (down to ∼7%) is indicative of strong sintering of the cupric phase. The three other modified supports provide substantial stabilization of a rather disperse and thermally stable cupric phase (Table 4).

In general, quantitative results obtained by ESR agree very well with the information obtained by FT-IR. Relying on all the data mentioned above, we selected three samples with substantially different properties of the dispersed cupric phase for a further comparative study of catalytic activity in ethane oxidation. They are: (1) Cu/MCM-41, with mainly thermally stable small irregular cupric clusters; (2) Cu/Al-MCM-41, with mainly thermally stable isolated Cu^{2+}-sites; (3) Cu/W-MCM-41 with a mixture of isolated and aggregated cupric states and low thermal stability.

3.4. Catalytic testing

Copper sites demonstrate catalytic activity in different oxidation reactions. In our case, ethane oxidation was chosen as a reliable test-reaction used earlier in our study of zeolite-supported copper.

The catalytic activity of pure MCM-41 is negligible up to 500 °C. Activities of copper-containing samples reach a steady-state within 15–20 min on stream and no drop in effectiveness of the catalysts is noted after 2 h of continuous use. The onset of partial oxidation becomes measurable at $T > 500$–520 °C on the less active samples.

The conversion of ethane on the samples Cu/MCM-41, Cu/Al-MCM-41, and Cu/W-MCM-41 calcined at different temperatures is presented in Fig. 8a–c, respectively, as a function of temperature. It is seen from Fig. 8 that activities of the samples differ sharply, especially after high-temperature treatment, and direct comparison of all experimental data at one fixed temperature is possible at a temperature (∼600 °C) when the conversion becomes too high for the more active samples. Therefore, we plotted our data in the coordinates of Arrhenius equation and extrapolated the results to 500 °C, i.e. to conditions of very low conversion, as done in previous work [28,29]. The reaction rates calculated at this fixed temperature, as turnover numbers per 1 surface Cu^{2+} ion, are presented in Table 5.

The results demonstrate how much the intrinsic catalytic activity, per one Cu^{2+}-active site accessible to the reactants,

Table 5
Specific activities of the Cu^{2+}-ions in complete oxidation of ethane

Sample	Turnover number at 500 °C, molecules C_2H_4 per 1 surface Cu^{2+} site per min	
	Calcined 520 °C, 4 h	Calcined 750 °C, 1 h
1% Cu/MCM-41	0.42	0.11
1% Cu/Al-MCM-41	0.063	0.0044
1% Cu/W-MCM-41	0.055	0.0040
0.5% Cu/H-ZSM-5	0.37	0.0171

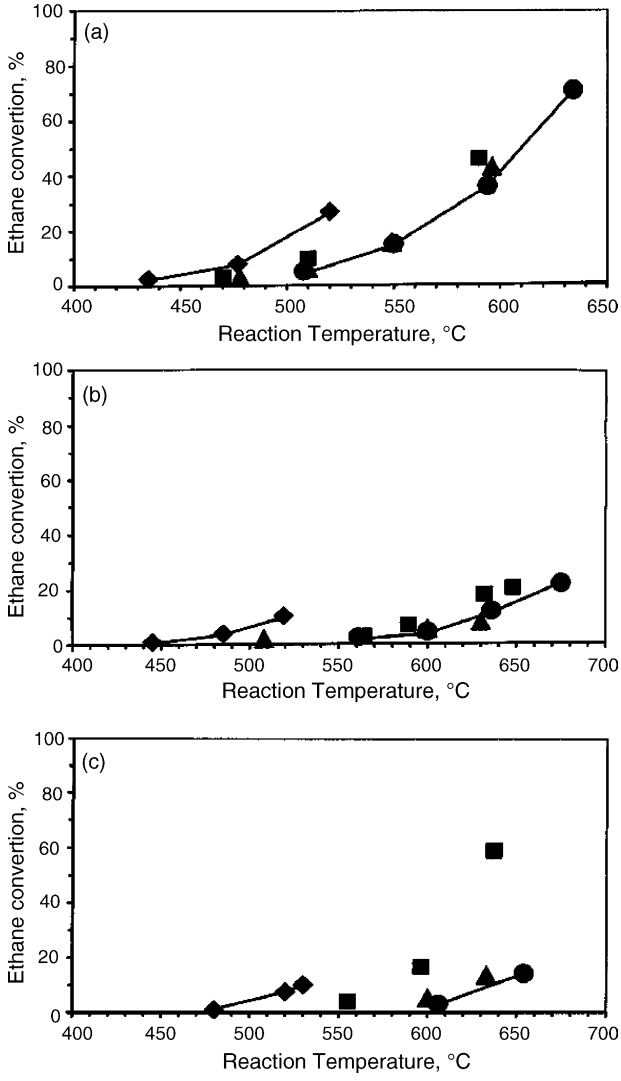

Fig. 8. Catalytic activity in ethane oxidation: (a) 1% Cu/MCM-41; (b) 1% Cu/Al-MCM-41; (c) 1% Cu/W-MCM-41. Calcination at (◆) 520 °C, 4 h; (■) 650 °C, 1 h; (▲) 650 °C, 3 h; (●) 750 °C, 1 h.

depends on the local site structure. Less disperse cupric phase in non-modified MCM-41 (weakly interacting Cu^{2+} ions in small defect clusters) has the highest intrinsic catalytic activity combined with a high thermal stability. Isolated, five-coordinated Cu^{2+}-sites grafted to Al-MCM-41 by calcination at 520 °C show substantially lower specific activity in total ethane oxidation. Thermal treatment at 650–750 °C causes no loss of accessible cupric ions but results in a ∼20-fold loss of the *specific* activity of Cu^{2+} catalytic sites of Cu/Al-MCM-41. As to Cu/W-MCM-41, a combined loss of both the number and of specific activity of Cu^{2+}-sites is observed after calcination. The results obtained are going in line with data demonstrating the lack of correlation between the dispersion of the Cu^{2+}-sites in modified MCM-41 and their catalytic activity [25,52,53].

A sample of Cu/HZSM-5 was tested for comparison under identical conditions (Table 5). It seems improper to compare the absolute turnover numbers for two supports differing so much in channel size and geometry. However, Cu/HZSM-5 exhibits the same, and even stronger, effect caused by calcination as

does Cu/Al-MCM-41: the structural rearrangement of coordinatively unsaturated isolated Cu^{2+}-sites leads to a sharp loss of the intrinsic activity of catalytic sites in ethane oxidation, as was shown previously [28,29,54].

4. Conclusions

It is possible to anchor to the surface of mesoporous silicates catalytically active, dispersed cupric ions. The dispersion, the thermal stability and the catalytic activity of these ions can be regulated by modification/grafting of the surface of the silicate by other ions.

The surface forms of Cu^{2+}-sites being accessible to water molecules can be quantified by ESR. Hydration shells effectively separate coupled paramagnetic ions or weaken the spin–lattice interaction of Cu^{2+} with the MCM-41 framework. Thus, a comparison with the frozen standard permits a selective quantitation of Cu^{2+}-active sites on the surface of MCM-41 supports.

No simple correlation exists between the total number of surface Cu^{2+}-sites on MCM-41 supports and catalytic activity in the total oxidation of ethane. The cupric sites on the aluminum-modified support have the highest dispersion and relatively high catalytic activity, but the less disperse copper on the non-modified MCM-41 has a higher specific catalytic activity which is also less susceptible to treatment at high temperatures.

Acknowledgment

A.V. Kucherov thanks SRL of Ford Motor Company for the use of the ESR spectrometer.

References

[1] A. Stein, B.J. Melde, R.C. Schroden, Adv. Mater. (Weinheim, Germany) 12 (19) (2000) 1403.
[2] (a) A. Corma, D. Kumar, Stud. Surf. Sci. Catal. 117 (1998) 201 (Mesoporous Molecular Sieves);
(b) A. Corma, D. Kumar, NATO ASI Ser. Ser. C 498 (1997) 403 (New Trends in Materials Chemistry).
[3] A. Sayari, Stud. Surf. Sci. Catal. 102 (1996) 1 (Recent Advances and New Horizons in Zeolite Science and Technology).
[4] A.A. Slinkin, A.V. Kucherov, Catal. Today 36 (1997) 485.
[5] A.V. Kucherov, H.G. Karge, R. Schlogl, Micropor. Mesopor. Mater. 25 (1–3) (1998) 7.
[6] A.V. Kucherov, S.G. Lakeev, M. Shelef, Appl. Catal. B 16 (1998) 245.
[7] A.V. Kucherov, A.A. Slinkin, M. Shelef, Catal. Lett. 50 (1998) 1.
[8] A.V. Kucherov, T.N. Kucherova, A.A. Slinkin, Micropor. Mesopor. Mater. 26 (1998) 1.
[9] A.V. Kucherov, C.N. Montreuil, T.N. Kucherova, M. Shelef, Catal. Lett. 56 (1998) 173.
[10] A.V. Kucherov, A.N. Shigapov, A.A. Ivanov, M. Shelef, J. Catal. 186 (1999) 334.
[11] A.V. Kucherov, M. Shelef, J. Catal. 195 (2000) 106.
[12] C.M. Kowalchuk, J.F. Corrigan, Y. Huang, Micropor. Mesopor. Mater. 81 (2005) 211.
[13] M. Ghadiri, F. Farzaneh, M. Ghandi, M. Alizadeh, J. Mol. Catal. A: Chem. 233 (2005) 127.
[14] Youzhu Yuan, Wei Cao, Weizheng Weng, J. Catal. 228 (2004) 311.
[15] She-T. Wong, Chia-H. Lee, Tien-S. Lin, Chung-Y. Mou, J. Catal. 228 (2004) 1.
[16] V. Ayala, A. Corma, M. Iglesias, F. Sanchez, J. Mol. Catal. A: Chem. 221 (2004) 201.
[17] P. Karandikar, K.C. Dhanya, S. Deshpande, A.J. Chandwadkar, S. Sivasanker, M. Agashe, Catal. Commun. 5 (2004) 69.
[18] M.J. Alcón, A. Corma, M. Iglesias, F. Sánchez, J. Mol. Catal. A: Chem. 194 (2003) 137.
[19] Shan Zheng, Lian Gao, Jinkun Guo, J. Solid State Chem. 152 (2000) 447.
[20] W. Böhlmann, K. Schandert, A. Pöppl, H.-C. Semmelhack, Zeolites 19 (1997) 297.
[21] Ying Wan, Jianxin Ma, Zheng Wang, Wei Zhou, S. Kaliaguine, J. Catal. 227 (2004) 242.
[22] V. Nieminen, N. Kumar, J. Datka, J. Päivärinta, M. Hotokka, E. Laine, T. Salmi, D.Yu. Murzin, Micropor. Mesopor. Mater. 60 (2003) 159.
[23] Qiang Wu, Xijun Hu, Po Lock Yue, Xiu Song Zhao, Gao Q. Lu, Appl. Catal. B: Environ. 32 (2001) 151.
[24] Xijun Hu, Frank L.Y. Lam, Lok M. Cheung, Ka F. Chan, Xiu S. Zhao, Gao Q. Lu, Catal. Today 68 (2001) 129.
[25] M. Ziolek, I. Sobczak, I. Nowak, P. Decyk, A. Lewandowska, J. Kujawa, Micropor. Mesopor. Mater. 35–36 (2000) 195.
[26] W.A. Carvalho, M. Wallau, U. Schuchardt, J. Mol. Catal. A: Chem. 144 (1999) 91.
[27] G. Grubert, J. Rathousky, G. Schulz-Ekloff, M. Wark, A. Zukal, Micropor. Mesopor. Mater. 22 (1998) 225.
[28] A.V. Kucherov, T.N. Kucherova, A.A. Slinkin, Catal. Lett. 10 (1991) 289.
[29] A.V. Kucherov, C.P. Hubbard, T.N. Kucherova, M. Shelef, Appl. Catal. B: Environ. 7 (1996) 285.
[30] J.S. Beck, J.C. Vartuli, W.J. Roth, M.E. Leonowicz, C.T. Kresge, K.D. Schmit, C.T.-W. Chu, D.H. Olson, E.W. Sheppard, S.B. McCullen, J.B. Higgins, J.L. Schlenker, J. Am. Chem. Soc. 114 (1992) 10834.
[31] J. Szanyi, M.T. Paffett, J. Chem. Soc., Faraday Trans. 92 (1996) 5165.
[32] A.V. Ivanov, G.W. Graham, M. Shelef, Appl. Catal. B: Environ. 21 (1999) 243.
[33] T. Tsoncheva, Tz. Venkov, M. Dimitrov, C. Minchev, K. Hadjiivanov, J. Mol. Catal. A: Chem. 209 (2004) 125.
[34] K. Hadjiivanov, T. Tsoncheva, M. Dimitrov, C. Minchev, H. Knözinger, Appl. Catal. A: Gen. 241 (2003) 331.
[35] N. Sheppard, T.T. Nguyen, Adv. Infrared Raman Spectr. 5 (1978) 67.
[36] S.F. Tikhov, E.A. Paukshtis, V.A. Sadykov, V.V. Popovskii, T.G. Starostina, G.N. Kriukova, G.V. Harlamov, V.F. Anufrienko, V.F. Poluboiarov, V.A. Pazdodarov, N.N. Bulgakov, A.V. Kalinkin, Kinet. Katal. 30 (1989) 869.
[37] K. Hadjiivanov, H. Knözinger, Phys. Chem. Chem. Phys. 3 (2001) 1132.
[38] D. Scarano, S. Bordiga, C. Lamberti, G. Spoto, G. Richiardi, A. Zecchina, C. Otero Arean, Surf. Sci. 411 (1998) 272.
[39] A. Dandekar, M.A. Vannice, Appl. Catal. B 22 (1999) 179.
[40] C. Lamberti, S. Bordiga, A. Zeccina, M. Salvalaggio, F. Geobaldo, C. Otero Arean, J. Chem. Soc., Faraday Trans. 94 (1998) 1519.
[41] H. Miessner, H. Landmesser, N. Jaeger, K. Richter, J. Chem. Soc., Faraday Trans. 93 (1997) 3417.
[42] G. Spoto, S. Bordiga, D. Scarano, A. Zeccina, Catal. Lett. 13 (1992) 29.
[43] J. Dedecek, Z. Sobalik, Z. Tvaruzkova, D. Kaucky, B. Wichterlova, J. Phys. Chem. 99 (1995) 16327.
[44] J. Szanyi, M.T. Paffett, J. Catal. 164 (1996) 232.
[45] A.A. Davydov, IR-spectroscopy in Chemistry of Oxide Surfaces, Nauka SB, Novosibirsk, 1984.
[46] M. Hartmann, Stud. Surf. Sci. Catal. 128 (2000) 215 (Characterization of Porous Solids V).
[47] S. Velu, L. Wang, M. Okazaki, K. Suzuki, S. Tomura, Micropor. Mesopor. Mater. 54 (2002) 113.
[48] J.-S. Yu, J.Y. Kim, L. Kevan, Micropor. Mesopor. Mater. 40 (2000) 135.
[49] A. Poppl, P. Baglioni, L. Kevan, J. Phys. Chem. 99 (1995) 14156.
[50] A. Zecchina, D. Scarano, G. Spoto, S. Bordiga, C. Lamberti, G. Bellussi, Stud. Surf. Sci. Catal. 117 (1998) 343 (Mesoporous Molecular Sieves).
[51] J. Dedecek, N. Zikova, J. Cejka, Stud. Surf. Sci. Catal. 129 (2000) 235 (Nanoporous Materials II).
[52] M.R. Prasad, G. Kamalakar, S.J. Kulkarni, K.V. Raghavan, J. Mol. Catal. A: Chem. 180 (2002) 109.
[53] W.A. Carvalho, M. Wallau, U. Schuchardt, J. Mol. Catal. A: Chem. 144 (1999) 91.
[54] A.V. Kucherov, J.L. Gerlock, H.-W. Jen, M. Shelef, J. Catal. 152 (1995) 63.